

Blessing and Curse: How a Supercapacitor's Large Capacitance Causes its Slow Charging


Cheng Lian^{1,*}, Mathijs Janssen^{1,2,3}, Honglai Liu^{4,†} and René van Roij¹

¹*Institute for Theoretical Physics, Center for Extreme Matter and Emergent Phenomena, Utrecht University, Princetonplein 5, 3584 CC Utrecht, The Netherlands*

²*Max-Planck-Institut für Intelligente Systeme, Heisenbergstraße 3, 70569 Stuttgart, Germany*

³*Institut für Theoretische Physik IV, Universität Stuttgart, Pfaffenwaldring 57, 70569 Stuttgart, Germany*

⁴*State Key Laboratory of Chemical Engineering, School of Chemistry and Molecular Engineering, East China University of Science and Technology, Shanghai 200237, China*

 (Received 21 November 2019; accepted 15 January 2020; published 20 February 2020)

The development of novel electrolytes and electrodes for supercapacitors is hindered by a gap of several orders of magnitude between experimentally measured and theoretically predicted charging time scales. Here, we propose an electrode model, containing many parallel stacked electrodes, that explains the slow charging dynamics of supercapacitors. At low applied potentials, the charging behavior of this model is described well by an equivalent circuit model. Conversely, at high potentials, charging dynamics slow down and evolve on two relaxation time scales: a generalized RC time and a diffusion time, which, interestingly, become similar for porous electrodes. The charging behavior of the stack-electrode model presented here helps to understand the charging dynamics of porous electrodes and qualitatively agrees with experimental time scales measured with porous electrodes.

DOI: 10.1103/PhysRevLett.124.076001

In the electric energy storage domain, supercapacitors [Fig. 1(a)] have proven their value in applications requiring higher power output than delivered by batteries and more energy than stored in dielectric capacitors [1–4]. Many types of carbon-based materials have been used for the capacitor's electrodes [5–7]. However, the relation between the porous structures and the charging dynamics of macroscopic supercapacitors is poorly understood. On the one hand, transmission line (TL) models [8–11] can successfully fit experimental data, but the fit parameters therein do not have a direct interpretation in terms of microscopic properties of supercapacitors. On the other hand, molecular dynamics simulation [12–18], lattice Boltzmann simulations [19,20], and classical dynamic density functional theory [21–23] can elucidate the charging mechanisms of a single or a few nanopores or a nanoscale anode-cathode model, but predicted relaxation time scales are of the order of ns, roughly 12 orders of magnitude smaller than experimentally measured 10^3 s timescales of supercapacitors [24–27]. These long charging times, however, can be decently approximated by multiplying a nanocapacitor's RC time by the squared ratio of nanocapacitor-to-supercapacitor thicknesses [14,18]. Even though such approaches to bridge scales are valuable, they ignore the actual multiscale character of the system, e.g., the transport of ions through quasineutral macropores. To faithfully describe the charging of supercapacitors, one should account for both the ionic currents from the ion reservoir that separates anode and cathode through a macropore network into the nanopores (micrometers) and for the

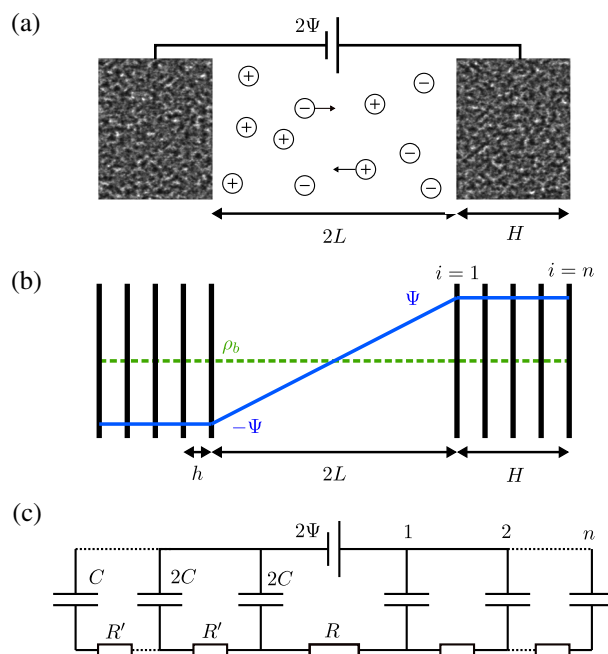


FIG. 1. (a) Sketch of a supercapacitor containing a 1:1 electrolyte, two porous electrodes, and a battery providing an electrostatic potential difference 2Ψ . (b) In our stack-electrode model, the cathode and anode each contain n planar electrodes at intervals of h . Initial anionic and cationic densities are ρ_b throughout the cell. At time $t = 0$, $-\Psi$ and $+\Psi$ are applied to all electrodes on the left and right-hand sides of the system, respectively. (c) Equivalent circuit model for the stack-electrode model.

electric double layer (EDL) buildup therein (nanometers). Clearly, such a multiscale analysis cannot be performed with the above mentioned simulation techniques alone, as computational power limits simulations to nanoscale systems. In this Letter, we present a minimal model to explain the long experimental relaxation timescales of supercapacitors, instead.

The canonical model describing ionic charge relaxation to an applied electric field employs a dilute 1:1 electrolyte and two parallel and planar blocking electrodes separated by a distance $2L$ [28]. Suddenly applying a potential difference 2Ψ with a battery, the two electrodes will acquire opposite surface charge densities $\pm e\sigma(t)$, eventually screened in the electrolyte by two EDLs, whose equilibrium width is characterized by the Debye length $\kappa^{-1} = \sqrt{\epsilon k_B T / 2e^2 \rho_b}$, with $2\rho_b$ the bulk ion number density, ϵ the electrolyte permittivity, e the elementary charge, and $k_B T$ the thermal energy. At late times and for $\kappa L \gg 1$, $\sigma(t) = 2\Phi \rho_b \kappa^{-1} [1 - \exp(-t/\tau_{RC})]$, with $2\Phi = 2e\Psi/k_B T$ the dimensionless applied potential, $\tau_{RC} = \kappa^{-1} L/D$ the RC time, and D the ionic diffusion coefficient [28–30]. Inserting typical experimental parameters $\kappa^{-1} \approx 1$ nm, $L \approx 250$ μm , and $D \approx 1 \times 10^{-9}$ $\text{m}^2 \text{s}^{-1}$ yields $\tau_{RC} \approx 10^{-4}$ s: larger than the timescales predicted by molecular simulations, but still 5 orders of magnitude smaller than the experimental charging time of supercapacitors. This discrepancy comes as no surprise as the above $\sigma(t)$ applies to planar electrodes: this model does not account for the huge surface area and for the ion transport through the porous structure of the supercapacitor electrodes. Simple extensions of the flat electrode setup were discussed, such as spherical and cylindrical electrodes [20,31] and a single cylindrical pore in contact with a reservoir [9]. Several theoretical works focused on the charging dynamics of porous electrodes [32–38]. Still, the gap between experimental and theoretical supercapacitor charging timescales has not been bridged yet.

To explain why the charging time of macroscopic porous electrodes [Fig. 1(a)] is much larger than that of flat electrodes, in this Letter, we will characterize the charging dynamics of the model shown in Fig. 1(b) and also compare it to the charging dynamics of the circuit shown in Fig. 1(c). In our model, the nanoporous cathode and anode of a supercapacitor are both modeled by a stack of n parallel electrodes with an equal spacing h mimicking the pore size, such that the thickness of the cathode and anode equals $H = (n-1)h$. The surface area A of all individual electrodes is assumed to be sufficiently large that we can ignore edge effects and study all microscopic observables as a function of a single coordinate x perpendicular to the electrode surfaces. We adopt a coordinate system whose origin lies in the middle ($x=0$) of the system and where the i th cathode and anode, with $i = \{1, \dots, n\}$, are located at $X_i = \pm[L + (i-1)h]$. All parallel stacked electrodes are fully permeable to the electrolyte in order to mimic the

porosity of supercapacitor electrodes, except the two outer ones ($i=n$) which are impermeable to have a closed system [cf. Eq. (2b)]. Thus, the ionic number densities $\rho_{\pm}(x, t)$ and ionic fluxes $j_{\pm}(x, t)$ are continuous at each X_i . Initially, the ionic number densities are homogenous

$$\rho_{\pm}(x, t=0) = \rho_b, \quad |x| \leq L + H. \quad (1)$$

At time $t=0$, a dimensionless potential difference 2Φ is applied to the macroscopic cathode and anode. This yields the following boundary conditions for $t > 0$:

$$\phi(\pm X_i, t) = \pm\Phi; \quad (2a)$$

$$j_{\pm}(\pm X_n, t) = 0, \quad (2b)$$

with $\phi(x, t)$ the electric potential in units of the thermal voltage $k_B T/e$. To model the ionic dynamics, we use the classical Poisson-Nernst-Planck (PNP) equations [28]

$$\partial_x^2 \phi(x, t) = -\kappa^2 \left[\frac{\rho_+(x, t) - \rho_-(x, t)}{2\rho_b} \right]; \quad (3a)$$

$$\partial_t \rho_{\pm}(x, t) = -\partial_x j_{\pm}(x, t); \quad (3b)$$

$$j_{\pm}(x, t) = -D[\partial_x \rho_{\pm}(x, t) \pm \rho_{\pm}(x, t) \partial_x \phi(x, t)]. \quad (3c)$$

In Eqs. (1)–(3) appear the applied potential Φ and four length scales: h , H , L , and κ^{-1} . With these parameters, we can construct many different combinations that yield $1 + 3$ independent dimensionless parameters, for instance: Φ , κL , κH , and κh or, equivalently, Φ , κL , H/L , and n . Here, we focus on the latter choice and mostly restrict to $H/L = 1$, which is reasonable for supercapacitors.

In Fig. 2(a), we present numerical results for $\phi(x, t)$ for a low potential $\Phi = 0.001$ and $\kappa L = 100$, $H/L = 1$, and $n = 5$. These parameters correspond to $\kappa h = 25$, which means that the EDLs are thin compared to the electrode separations. Initially, the potential in the reservoir ($|x| < L$) displays a typical linear x dependence, which corresponds to a spatially constant electric field. At later times, the potential retains this linear dependence in the reservoir, albeit with a slope that decreases with time due to the buildup of EDLs. At short times $t/\tau_{RC} \leq 20$, there is a clear asymmetry between the two EDLs that surround individual planar electrodes. This asymmetry is lost at later times $t \geq 20\tau_{RC}$, when the EDLs fully equilibrate.

For the same parameters, in Fig. 2(b), we show the surface charge densities $e\sigma_i$ of the individual electrodes (labeled with i), which we find with Gauss' law $\sigma_i(t) = -2\rho_b \kappa^{-2} [\partial_x \phi|_{X_i^+} - \partial_x \phi|_{X_i^-}]$. At early times $t < \tau_{RC}$, the electrodes charge faster the closer they are situated to the reservoir, $\sigma_1 > \sigma_2 > \dots > \sigma_n$. However, the late-time relaxation timescale is the same for all electrodes: all electrodes reach 99.9% of their equilibrium charge around

$t/\tau_{RC} \approx 50$. As the outer electrodes face the electrolyte only at one side, we have $\partial_x \phi|_{x_n^+} = \partial_x \phi|_{-x_n^-} = 0$, and $\sigma_n(t/\tau_{RC} \rightarrow \infty)$ is a factor two smaller than the surface charge density of the other electrodes. To better understand these phenomena, we studied the behavior of the circuit model shown in Fig. 1(c). Note the great similarity of this model to traditional TL models used for fitting experimental data: the only difference is the capacitance C of the outermost capacitor, rather than $2C$ in the TL model [39]. However, in contrast to the TL model, where R , C , and n are fit parameters, the elements of the circuit in Fig. 1(c) are all one-to-one related to electrolyte and electrode properties of our microscopic model, $R = 2L/(A\epsilon\kappa^2D)$ and $C = A\epsilon\kappa$. In the Supplemental Material [39], we derive a matrix differential equation [cf. Eq. (S11)] that relates the potential drops over the n capacitors to the currents through the n resistors. With the solution to this equation, we find predictions for the time-dependent charge on each capacitor in this circuit, which translates into a prediction for $\sigma_i(t)$ in the corresponding microscopic model, shown in Fig. 2(b) with symbols [39]. Clearly, the predictions from the microscopic and circuit model are indistinguishable. In line with our earlier observation, the equivalent-circuit model predicts that all electrodes relax exponentially at late times with the same time constant τ_n

$$\frac{\tau_n}{\tau_{RC}} = \left(2 + 0.75 \frac{H}{L}\right)n - 1 - 0.91 \frac{H}{L}, \quad (4)$$

which correctly reduces to $\tau_1 = \tau_{RC}$ for $n = 1$ (for which $H/L = 0$), the coefficients 2 and 1 appearing in Eq. (4) are analytical results obtained in the limit $H/L \rightarrow 0$; the other numerical factors relate to the smallest eigenvalue of an almost-Toeplitz matrix in the afore-mentioned matrix differential equation. From Eq. (4), we see that τ_n is large whenever n is large. This suggests that the large relaxation time of supercapacitors stems from their large internal surface area, achieved through many small pores. Interestingly, Eq. (4) recovers the electronic circuit intuition

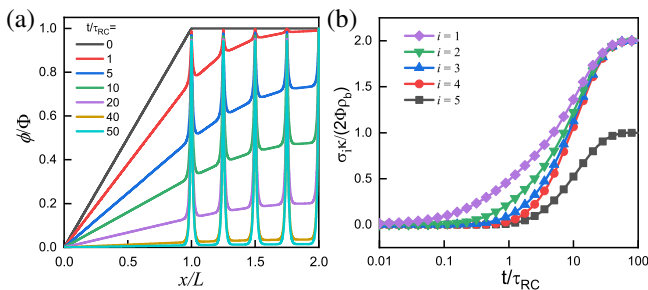


FIG. 2. Time dependence of the scaled (a) potential $\phi(x, t)$ and (b) the surface charge densities $\sigma_i(t)$ for $i = \{1, \dots, 5\}$ of the electrode for $\Phi = 0.001$, $\kappa L = 100$, $H/L = 1$, and $n = 5$. The symbols and lines in (b) correspond to numerical and equivalent-circuit model calculations, respectively.

that a supercapacitor should charge slower the larger its electrode surface area. This areal scaling is not present in the relaxation time τ_{RC} of Ref. [28] as, in that work, R and C scale oppositely with A .

Because supercapacitors are typically subjected to large potentials in practical applications, we also characterize the dynamics of the stack-electrode model at $\Phi > 1$. In Figs. 3(a), 3(c), and 3(e) we present data for $\Phi = \{0.01, 0.1, 1, 2\}$, $\kappa L = 100$, and $n = 1$ (hence, $H/L = 0$). For this two-electrode setup, it is known that, next to τ_{RC} , the diffusion time L^2/D emerges in the ionic relaxation due to slow salt diffusion from the cell center to the electrode surfaces [28,30,43]. Indeed, Fig. 3(a) shows that the normalized surface density $\sigma_n(t)/\sigma_{eq}$, with $\sigma_{eq} \equiv \sigma_n(t/\tau_{RC} \rightarrow \infty)$ the late-time surface charge density, develops slower at higher Φ . Next, Fig. 3(c) shows the salt concentration at the cell center $c(t) = [\rho_+(0, t) + \rho_-(0, t)]/(2\rho_b)$ for the same Φ . We see that $c(t) \approx 1$ for $\Phi \leq 0.1$ and that $c(t)$ decreases at late times ($t/\tau_{RC} > 10$) by 0.25% and 1% for $\Phi = 1$ and 2: As our setup is closed, a net ionic adsorption on the electrodes “desalinates” the cell center [44]. To investigate the emergence of the slow timescale at large applied potentials, in Fig. 3(e), we show the charge relaxation $1 - \sigma(t)/\sigma_{eq}$ (solid lines) and the concentration decay $[c(t) - c_{eq}]/(1 - c_{eq})$ (dashed lines), where $c_{eq} \equiv c(t/\tau_{RC} \rightarrow \infty)$. At early times ($t/\tau_{RC} < 1$), all data for $1 - \sigma(t)/\sigma_{eq}$ collapse onto the $\Phi = 0.01$ curve, indicating that the initial ionic relaxation is described well by the equivalent circuit model, even for higher Φ . Thereafter, a second, slower relaxation emerges in $1 - \sigma(t)/\sigma_{eq}$, emerging more dominantly for higher Φ . At late times, the slopes of $1 - \sigma(t)/\sigma_{eq}$ and $[c(t) - c_{eq}]/(1 - c_{eq})$ are the same. Numerical results [cf. Fig. S7(d) of the Supplemental Material [39]] for the adsorption timescale τ_{ad} , the inverse of these slopes, show that τ_{ad}/τ_{RC} is independent of Φ (for all Φ considered) and scales linearly with κL . Using the definition of τ_{RC} , we then recover the L^2/D scaling of τ_{ad} suggested by Refs. [28,30]. To check the robustness of our findings, we performed dynamical density functional theory calculations of a room temperature ionic liquid at the experimental voltage $\Psi = 0.5$ V [39]. Interestingly, the surface charge again shows two distinct relaxation processes.

To investigate the effect of $n > 1$ for high potentials, in Figs. 3(b), 3(d), and 3(f), we plot the same observables as in Figs. 3(a), 3(c), and 3(e), now for $\Phi = 2$, $\kappa L = 100$, $H/L = 1$, and $n = \{2, 3, 6\}$. Similar to our $\Phi = 0.001$ findings [condensed in τ_n of Eq. (4)], we see that the charging dynamics at $\Phi = 2$ also slows down with increasing n . The salt concentration at the cell center $c(t)$ [Fig. 3(d)] is again unaffected at early times $t/\tau_{RC} < 5$, after which it decays to an equilibrium value that decreases with n . Thus, our model recovers the

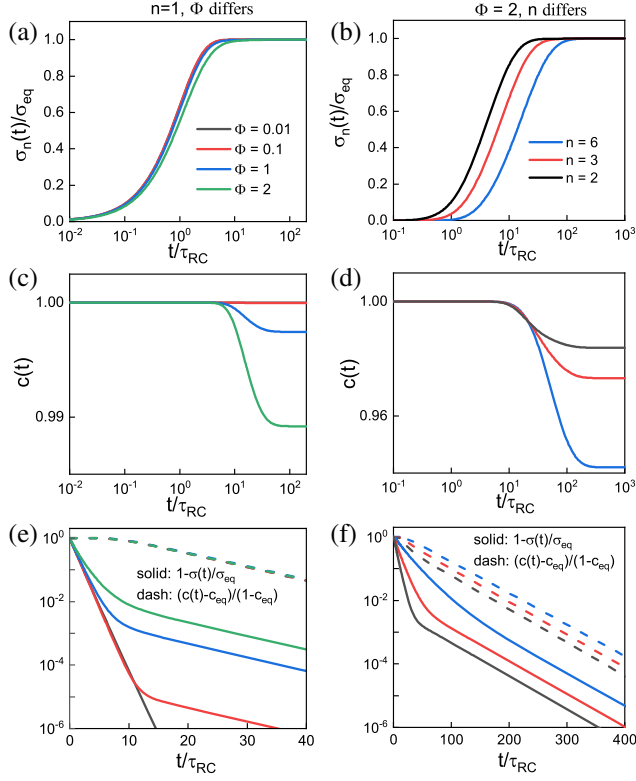


FIG. 3. The surface charge density (a), (b) $\sigma(t)/\sigma_{eq}$, the salt concentration at the cell center (c), (d) $c(t)$, and the charge relaxation (e), (f) $1 - \sigma(t)/\sigma_{eq}$ (solid lines) and the concentration decay $[c(t) - c_{eq}]/[c(0) - c_{eq}]$ (dashed lines) of the stack-electrode model for $\kappa L = 100$, in (a), (c), and (e) for $n = 1$, $H/L = 0$ at potentials $\Phi = \{0.01, 0.1, 1, 2\}$, and in (b), (d), and (f) for $\Phi = 2$ and $H/L = 1$, at $n = \{2, 3, 6\}$.

intuition that, for two electrodes of the same volume, the one with more pores (and, hence, a large surface area) desalinates an electrolyte reservoir more. In Fig. 3(f), we see that the surface charge again decays on two distinct timescales. Plotting the same data with time scaled by τ_n instead of by τ_{RC} [cf. Fig. S8(c) of the Supplemental Material [39]], all $1 - \sigma(t)/\sigma_{eq}$ collapse for $t \leq \tau_n$, which shows that the circuit model decently describes the early-time relaxation at high potentials as well. Conversely, at late times, we see in Fig. 3(f) that $1 - \sigma(t)/\sigma_{eq}$ and $[c(t) - c_{eq}]/(1 - c_{eq})$ decay exponentially with a time constant τ_{ad} that does not depend on n for the parameter set under consideration. Considering a larger set of κL , κh , and n , we show τ_{ad} in Fig. 4(a). From this figure we conclude that

$$\tau_{ad} = \alpha \frac{(H + L)^2}{D}, \quad (5)$$

hence, the adsorption time τ_{ad} depends on the total system size. We show the κh -dependent prefactor α in Fig. 4(b) for various κL , which reveals that α is κL independent and that

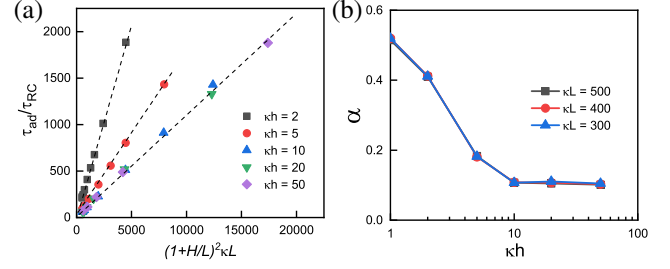


FIG. 4. (a) The dependence of the (scaled) adsorption timescale τ_{ad} on the (scaled) system size $(L + H)^2$ for $\kappa L = 500$ at potential $\Phi = 2$ at several pore sizes $\kappa h = \{2, 5, 10, 20, 50\}$ and $n = \{2, 5, 10, 20, 50, 100, 150, 200, 300\}$, with $n = 200$ and $n = 300$ for $\kappa h = 20$ and $\kappa h = 50$ off the scale of the plot. (b) The prefactor α of [Eq. (5)] as a function of κh for $\kappa L = 500$ with a linear fit through the data in (a); $\kappa L = 300$ and 400 with identical results.

$\alpha \approx 0.1$ for $\kappa h > 10$, while α increases with decreasing $\kappa h \leq 10$.

Since τ_n [Eq. (4)] and τ_{ad} [Eq. (5)] depend on κL , κh , and n differently, both $\tau_{ad}/\tau_n \ll 1$, $\tau_{ad}/\tau_n \approx 1$, and $\tau_{ad}/\tau_n \gg 1$ are possible. Focusing here on $n \gg 1$, which is relevant to macroscopic electrodes, we find

$$\frac{\tau_n}{\tau_{ad}} \approx \begin{cases} \frac{0.75 H}{\alpha \kappa h L} & L \gg H; \\ \frac{0.69}{\alpha \kappa h} & L = H; \\ \frac{2}{\alpha \kappa h L} & L \ll H. \end{cases} \quad (6)$$

For $H/L = 1$ (and $n \gg 1$), we find that $\tau_n/\tau_{ad} \sim 1$ whenever $\kappa h < 10$.

Finally, it is interesting to determine the applicability of our stack-electrode model to experiments: Here, we consider the setup of Ref. [26], where two carbon electrodes of thickness $H = 0.5$ mm, separation $2L = 2.2$ mm, porosity $p = 0.65$, mass density $\rho = 5.8 \times 10^5$ g m $^{-3}$, and Brunauer-Emmett-Teller area $A_{BET} = 1330$ m 2 g $^{-1}$ were used. Assuming each porous electrode to consist of two flat solid carbon slabs, we get a crude estimate for the pore size with $h = p/(\rho A_{BET}) = 0.84$ nm. The electrodes were immersed in a 1 M NaCl solution at room temperature, hence, $\kappa^{-1} = 0.3$ nm and bulk diffusivity $D = 1.6 \times 10^{-9}$ m 2 s $^{-1}$. [We ignore that D is smaller in nanopores [32,41] and that different diffusivities may appear in Eqs. (4) and (5) [45]]. These parameters correspond, in our model, to $H/L = 0.45$, $n = 5.9 \times 10^5$, and $\kappa h = 2.8$, hence, $\alpha = 0.3$. With Eqs. (4) and (5), we now find $\tau_n = 2.9 \times 10^2$ s and $\tau_{ad} = 4.8 \times 10^2$ s, roughly within 1 order of magnitude from the two timescales (2×10^2 s and 9×10^3 s) observed in the experimental data of Ref. [26] (see Supplemental Material for details [39]). Given the simplicity of our model and crudeness of our estimates of κh , n , and D , the remaining discrepancies are not surprising. Yet, the stack-electrode model has bridged

the 5-orders-of-magnitude gap between experimental relaxation times and those predicted in the $n = 1$ model.

In summary, we studied the charging dynamics of nanoporous electrodes with a simple electrode model. At small applied potentials, numerical simulations of the PNP equations are reproduced accurately by an equivalent circuit model. This circuit model is akin to TL models used often to fit experimental supercapacitor data. Notably, however, the resistances, capacitances, and number of branches in the circuit model are not fit parameters but physically determined by our microscopic model. This one-to-one relation allows us to interpret the long relaxation time of supercapacitors as being due to a large number n of pores in nanoporous electrodes: The stack-electrode model relaxes with the timescale $\tau_n \sim (2 + 0.75H/L)n\tau_{RC}$. At higher potentials, the surface charge still relaxes at early times with τ_n . Higher potentials also lead to slow salt adsorption in the EDLs and concomitant depletion of the reservoir on the timescale $\tau_{ad} \sim (L + H)^2/D$. As salt and charge transport are coupled, the long timescale τ_{ad} also governs the late-time surface charge relaxation, all the more so the higher the applied potential. The two timescales τ_n and τ_{ad} differ orders of magnitude for small n but become similar when electrodes have many pores, as is the case for supercapacitors. Inserting parameters relating to a recent experimental study [26], our simple model predicts the two observed relaxation times roughly within 1 order of magnitude. Thus, our model successfully bridged the 5-orders-of-magnitude gap between theoretically predicted and experimentally measured timescales, and could serve as a basis for extensions that break the planar symmetry. However, more work is needed to fully understand the charging dynamics of porous electrodes, which should include effects due to finite ion sizes, more realistic modeling of pore morphology, Faradaic reactions, position-dependent diffusion coefficients, etc.

This work is part of the D-ITP consortium, a program of the Netherlands Organisation for Scientific Research (NWO) that is funded by the Dutch Ministry of Education, Culture and Science (OCW). C. L. and R. v. R. acknowledge the EU-FET Project NANOPHLOW (No. REP-766972-1), M. J. acknowledges support from S. Dietrich, and H. L. acknowledges NSFC (Grants No. 91834301 and No. 21808055). We kindly thank Pieter Kouyzer for helpful discussions, Ben Ern e for access to the experimental data of Ref. [26], and Sviatoslav Kondrat for comments on our manuscript. C. L. and M. J. contributed equally to this work.

* c.lian@uu.nl

† hlliu@ecust.edu.cn

[1] J. Chmiola, G. Yushin, Y. Gogotsi, C. Portet, P. Simon, and P.-L. Taberna, *Science* **313**, 1760 (2006).

- [2] D. T. Limmer, C. Merlet, M. Salanne, D. Chandler, P. A. Madden, R. van Roij, and B. Rotenberg, *Phys. Rev. Lett.* **111**, 106102 (2013).
- [3] A. C. Forse, J. M. Griffin, C. Merlet, J. Carretero-Gonzalez, A.-R. O. Raji, N. M. Trease, and C. P. Grey, *Nat. Energy* **2**, 16216 (2017).
- [4] C. Prehal, C. Koczwara, H. Amenitsch, V. Presser, and O. Paris, *Nat. Commun.* **9**, 4145 (2018).
- [5] P. Simon and Y. Gogotsi, *Acc. Chem. Res.* **46**, 1094 (2013).
- [6] C. Cheng, G. Jiang, C. J. Garvey, Y. Wang, G. P. Simon, J. Z. Liu, and D. Li, *Sci. Adv.* **2**, e1501272 (2016).
- [7] T. Mouterde, A. Keerthi, A. R. Poggioli, S. A. Dar, A. Siria, A. K. Geim, L. Bocquet, and B. Radha, *Nature (London)* **567**, 87 (2019).
- [8] R. de Levie, *Electrochim. Acta* **8**, 751 (1963).
- [9] M. Mirzadeh, F. Gibou, and T. M. Squires, *Phys. Rev. Lett.* **113**, 097701 (2014).
- [10] R. Tivony, S. Safran, P. Pincus, G. Silbert, and J. Klein, *Nat. Commun.* **9**, 4203 (2018).
- [11] L. Helseth, *J. Energy Storage* **25**, 100912 (2019).
- [12] G. Feng and P. T. Cummings, *J. Phys. Chem. Lett.* **2**, 2859 (2011).
- [13] S. Kondrat, P. Wu, R. Qiao, and A. A. Kornyshev, *Nat. Mater.* **13**, 387 (2014).
- [14] C. P an, C. Merlet, B. Rotenberg, P. A. Madden, P.-L. Taberna, B. Daffos, M. Salanne, and P. Simon, *ACS Nano* **8**, 1576 (2014).
- [15] K. Breitsprecher, C. Holm, and S. Kondrat, *ACS Nano* **12**, 9733 (2018).
- [16] G. Feng, M. Chen, S. Bi, Z. A. H. Goodwin, E. B. Postnikov, N. Brilliantov, M. Urbakh, and A. A. Kornyshev, *Phys. Rev. X* **9**, 021024 (2019).
- [17] C. Noh and Y. Jung, *Phys. Chem. Chem. Phys.* **21**, 6790 (2019).
- [18] S. Bi, M. Chen, R. Wang, J. Feng, M. Dinca, A. A. Kornyshev, and G. Feng, [arXiv:1903.00279](https://arxiv.org/abs/1903.00279).
- [19] A. Chatterji and J. Horbach, *J. Chem. Phys.* **126**, 064907 (2007).
- [20] A. J. Asta, I. Palaia, E. Trizac, M. Levesque, and B. Rotenberg, *J. Chem. Phys.* **151**, 114104 (2019).
- [21] C. Lian, S. Zhao, H. Liu, and J. Wu, *J. Chem. Phys.* **145**, 204707 (2016).
- [22] S. Babel, M. Eikerling, and H. L wen, *J. Phys. Chem. C* **122**, 21724 (2018).
- [23] J. Jiang, D. Cao, D.-e. Jiang, and J. Wu, *J. Phys. Chem. Lett.* **5**, 2195 (2014).
- [24] D. Brogioli, R. Zhao, and P. M. Biesheuvel, *Energy Environ. Sci.* **4**, 772 (2011).
- [25] C. Lian, K. Liu, K. L. van Aken, Y. Gogotsi, D. J. Wesolowski, H. L. Liu, D. E. Jiang, and J. Z. Wu, *ACS Energy Lett.* **1**, 21 (2016).
- [26] M. Janssen, E. Griffioen, P. M. Biesheuvel, R. van Roij, and B. H. Ern e, *Phys. Rev. Lett.* **119**, 166002 (2017).
- [27] A. S. Ambrozevich, S. A. Ambrozevich, R. T. Sibatov, and V. V. Uchaikin, *Russian Electrical Engineering* **89**, 64 (2018).
- [28] M. Z. Bazant, K. Thornton, and A. Ajdari, *Phys. Rev. E* **70**, 021506 (2004).
- [29] M. Janssen and M. Bier, *Phys. Rev. E* **97**, 052616 (2018).

- [30] I. Palaia, Ph.D. thesis, Université Paris-Saclay, 2019 (private communication).
- [31] M. Janssen, *Phys. Rev. E* **100**, 042602 (2019).
- [32] H. Sakaguchi and R. Baba, *Phys. Rev. E* **76**, 011501 (2007).
- [33] P. M. Biesheuvel and M. Z. Bazant, *Phys. Rev. E* **81**, 031502 (2010).
- [34] R. Zhao, O. Satpradit, H. H. M. Rijnaarts, P. M. Biesheuvel, and A. van der Wal, *Water Res.* **47**, 1941 (2013).
- [35] A. Obliger, M. Jardat, D. Coelho, S. Bekri, and B. Rotenberg, *Phys. Rev. E* **89**, 043013 (2014).
- [36] L. Pilon, H. Wang, and A. L. d'Entremont, *J. Electrochem. Soc.* **162**, A5158 (2015).
- [37] C. Lian, H. Su, C. Li, H. Liu, and J. Wu, *ACS Nano* **13**, 8185 (2019).
- [38] A. Eftekhari, *ACS Sustain. Chem. Eng.* **7**, 3692 (2019).
- [39] See Supplemental Material at <http://link.aps.org/supplemental/10.1103/PhysRevLett.124.076001> for a discussion of the relation between the TL model and our circuit model, for a derivation of Eq. (4), for PNP data at other parameter values, for dynamical density functional theory results at $n = 1$, and for a discussion of the relaxation timescales in the data of Ref. [26]. The Supplemental Material includes Refs. [23,26,32,40–42].
- [40] P. A. J. Kouzyer, Master's thesis, Utrecht University, 2015.
- [41] E. Allahyarov, H. Löwen, and P. L. Taylor, *Electrochim. Acta* **242**, 73 (2017).
- [42] M. A. Gebbie, A. M. Smith, H. A. Dobbs, A. A. Lee, G. G. Warr, X. Banquy, M. Valtiner, M. W. Rutland, J. N. Israelachvili, S. Perkin, and R. Atkin, *Chem. Commun. (Cambridge)* **53**, 1214 (2017).
- [43] L. Højgaard Olesen, M. Z. Bazant, and H. Bruus, *Phys. Rev. E* **82**, 011501 (2010).
- [44] N. Boon and R. van Roij, *Mol. Phys.* **109**, 1229 (2011).
- [45] M. Janssen and M. Bier, *Phys. Rev. E* **99**, 042136 (2019).